

Rowan University

Rowan Digital Works

Faculty Scholarship for the College of Science & Mathematics

College of Science & Mathematics

10-3-2022

Role of Draw Rate and Molecular Weight when Electrospun Nanofibers are Post-Drawn with Residual Solvent

Adriano Conte
Rowan University

Xiao Hu
Rowan University

Vincent Beachley
Rowan University, beachley@rowan.edu

Follow this and additional works at: https://rdw.rowan.edu/csm_facpub



Part of the [Physics Commons](#)

Recommended Citation

Conte, A. A., Hu, X., Beachley, V., Role of Draw Rate and Molecular Weight when Electrospun Nanofibers are Post-Drawn with Residual Solvent. *Macromolecular Materials & Engineering* 2022, 2200475.
<https://doi.org/10.1002/mame.202200475>

This Article is brought to you for free and open access by the College of Science & Mathematics at Rowan Digital Works. It has been accepted for inclusion in Faculty Scholarship for the College of Science & Mathematics by an authorized administrator of Rowan Digital Works.

Role of Draw Rate and Molecular Weight when Electrospun Nanofibers are Post-Drawn with Residual Solvent

Adriano A. Conte, Xiao Hu, and Vince Beachley*

The postdrawing process is poorly understood for polymer nanofibers due to the difficulty of manipulating nanofiber structures. Here, an angled track system facilitates postdrawing of individual nanofibers with control of parameters including molecular weight, draw rate, draw ratio, and solvent evaporation time. In this study, the effects of molecular weight, draw rate, and relative residual solvent content on final nanofiber properties are investigated. Molecular weight is first investigated to clarify any influence polymer chain length can have on drawing in facilitating or hindering chain extensibility. Polyacrylonitrile nanofibers with 50 and 150 kDa molecular weights behave similarly with postdrawing resulting in reduced diameters and enhanced mechanics. Since solvent quantity during drawing is a time sensitive component it is meaningful to assess the impact of draw rate on the chemical and structural makeup of postdrawn fibers. Chemical bond vibrations and chain orientation are sensitive to draw rate when polycaprolactone nanofibers are dried for 3 minutes prior to postdrawing, but this dependency to draw rate is not observed when fibers are postdrawn immediately upon collection. These findings demonstrate that the amount of retained solvent at collection is relevant to this postprocessing approach, and highlights the dynamics of solvent evaporation during postdrawing.

weight polymers result in higher mechanical strength materials, but these properties may also prevent optimal postdrawing.^[6,8] Literature describing conventionally spun fibers has demonstrated that post-drawing higher molecular weight polymers produces higher tensile strength^[10] although, more breakage tends to be present at higher elongations for higher molecular weights. A study of conventionally spun silk fibers showed that a higher molecular weight also resulted in a higher degree of crystallinity while a lower molecular weight demonstrated greater orientation factor.^[11] In response to these observations it is important to investigate any role molecular weight could play in the post-drawing of electrospun fibers. Furthermore, since higher molecular weight polymers will consist of increased chain lengths and tie molecules, these properties may help compliment the drawing process, allowing for greater extensibility of the chain segments.

In conventional microfiber spinning, the parameter of draw rate is difficult to decouple from the parameter of draw ratio

1. Introduction

Postdrawing is a common practice in conventional fiber manufacturing in which the effects of parameters such as draw rate, draw ratio, and molecular weight on the postdrawing process have been thoroughly investigated.^[1-9] Previous studies have shown that increased tie-molecules found in higher molecular

wherein draw ratio has normally been a ratio between the upstream and downstream take up roller speeds. Disregarding this common observation, it has been shown that high speed spinning of greater than 3500 m min⁻¹ may induce crystallization even within slowly crystallizing polymers such as PET.^[12] However excessively high speeds have resulted in diminished crystallinity with less crystallization time, reduced molecular alignment, and poor mechanical properties of resultant fibers produced.^[13] Experimental data has shown that there is an optimal draw rate and temperature in which drawing can occur due to time/temperature superposition principles for conventionally drawn fibers.^[14,15] Moreover, there was a calculated dependence of maximum draw ratio on draw rate such that a particularly narrow window of draw rates will result in a peak achievable draw ratio.^[16] Despite its importance, draw rate has yet to be studied with respect to individually drawn nanofibers. Further, since electrospun nanofibers contain residual solvent that is rapidly evaporating, draw rate is a vital aspect of the post-drawing process that is intrinsically tied to solvent content of the polymer. Being that solvent content is a time dependent attribute of electrospun fibers, this characteristic could possibly be modulated to produce various fiber morphologies and altered chemical structures through the means of controlling draw rate.

A. A. Conte, V. Beachley
 Department of Biomedical Engineering
 Rowan University
 Glassboro, NJ 08028, USA
 E-mail: beachley@rowan.edu

X. Hu
 Department of Physics and Astronomy
 Rowan University
 Glassboro, NJ 08028, USA

 The ORCID identification number(s) for the author(s) of this article can be found under <https://doi.org/10.1002/mame.202200475>

© 2022 The Authors. Macromolecular Materials and Engineering published by Wiley-VCH GmbH. This is an open access article under the terms of the Creative Commons Attribution License, which permits use, distribution and reproduction in any medium, provided the original work is properly cited.

DOI: 10.1002/mame.202200475

Carrying out such experiments on delicate polymer nanofibers presents significant challenges, but individual nanofiber post-drawing has recently been implemented in the electrospinning technique by using an automated collection system with two parallel facing, adjustable, and rotatable tracks.^[17] Individual nanofibers are elongated to several times their original length immediately following collection and thousands of individual electrospun nanofibers can be processed in minutes. In comparison to conventional extrusion based microfiber processing, this system is most similar to dry spinning.^[18] The original purpose of this implement was to postdraw individual nanofibers prior to complete solvent evaporation to facilitate postdrawing to higher draw ratios, and prevent the occurrences of polymer chain relaxation in electrospun fibers after collection.^[19–21] This added post-drawing process has allowed for diameter reduction, enhancement of strength,^[17,22] and enhancement of piezoelectric output.^[23] However, the effects of key parameters such as draw rate, molecular weight, and solvent content during electrospun nanofiber postdrawing with automated tracks remains uninvestigated.

2. Experimental Section

2.1. Electrospinning

All experiments were performed at room temperature (75–77 °C). Polyacrylonitrile (PAN, Sarchem Labs) at molecular weights of 50 000 and 150 000 Da were dissolved in dimethylformamide (DMF) at 18% w/v resulting in solutions with viscosities of 16738 ± 1017 and 20140 ± 927 cP, respectively. Solutions were fed through a 21-gauge blunt tipped needle at a feed rate of 0.8 mL h⁻¹, and electrospun using a voltage of 18 kV. Aligned nanofibers were collected using the automated tracks collection system. Under these conditions, PAN at various molecular weights was easily electrospun, but fibers had a tendency to peel off of the tracks at very high draw rates. Samples were drawn to a draw ratio (final length/initial length) of three (DR3) to allow for maximal drawing while preventing fiber breakage and peeling. An optimal relative humidity of $\approx 35\%$ was maintained within an environmental chamber containing the automated track device to limit observed PAN fiber peeling from the tracks.

For draw rate studies, electrospinning was performed using 18% w/v polycaprolactone (PCL, Sigma 80 000 M_n) dissolved in a 3 to 1 ratio of dichloromethane (DCM) and DMF. Solution was fed by a syringe pump at a rate of 0.8 mL h⁻¹ through a 21-gauge blunt tipped needle connected to a high voltage supply set to 6.5 kV. An optimal relative humidity of $\approx 60\%$ for electrospinning PCL was maintained within an environmental chamber containing the automated track device. A needle height above the collector was maintained at 9 cm. Under these conditions, PCL was difficult to spin at different molecular weights, but fibers could be drawn at high draw rates at up to a DR4 without observed breakage or peeling.

2.2. Fiber Collection and Processing with Automated Tracks

An automated device for postdrawing individual fibers consisted of an aluminum peg board where rollers could be attached in multiple locations to drive custom chainmail track

(wire-mesh.com, York, PA) configurations. Tracks were rotated by Nema stepper motors. The standard configuration (**Figure 1A**) had a 3.5 cm gap between the two tracks towards the top of the device, and a 33 cm gap between the tracks at the bottom. This configuration postdraws fibers immediately upon deposition when residual solvent content is maximal. Immediate post-drawing with maximum solvent content will be referred to as “wet.” Aligned electrospun nanofibers were collected across the top gap with one end adhered to each track. As the tracks pulled the fibers down they were postdrawn. An acrylic collection tray was placed at an appropriate height between both tracks for the collection of fibers at a draw ratio of DR3 (10.5 cm gap) or DR4 (14 cm gap). A programmable controller wired to the stepper motors was implemented for precise control of speed and ultimately the draw rate occurring during postdrawing. The programmable controller was set to a fixed low, medium, or high speed that resulted in linear draw rates of 0.0417, 0.303, or 1.489 cm s⁻¹ for draw rate assessments and 0.303 cm s⁻¹ for all molecular weight related studies. A second configuration (Delay – **Figure 1B**) was used to postdraw nanofibers at a draw ratio of DR4 (14 cm gap) after a time delay intended to allow for solvent evaporation. The postdrawing after a drying delay will be referred to as “dry.” Electrospun fibers were collected with the track in motion until they had filled the undrawn/drying region (straight portion of tracks). Then the tracks and the electrospinning process were stopped for 3 min, to allow solvent evaporation, followed by restarting the tracks at a fixed low, medium, or high speed that resulted in linear draw rates of 0.0764, 0.593, or 2.74 cm s⁻¹ to postdraw the suspended nanofibers to a draw ratio of DR4 at three different draw rates.

To evaluate fiber uniformity, samples were cut from the sides and center line of the fiber collection tray for PCL samples post-drawn with a draw rate of 0.0147 and 1.489 cm s⁻¹. Samples taken from the side were 0.5 cm from the tracks, while samples obtained from the center were within 1 cm of the centerline of the sample. Six replicates were analyzed for all groups ($n = 6$). A control group of undrawn fibers of the same sample size was produced by collecting fibers at the top of the tracks without drawing them. Samples were adhered between plastic window squares (inner dimension of 10 × 10 mm) and cut with a Silhouette Cameo for further characterization.

2.3. Imaging

A Phenom XL Desktop scanning electron microscope (SEM) was utilized to view gold sputter coated fiber morphology and quantify fiber diameter at a magnification 10 000×. A magnification of 1500× was set to observe the number of fibers per sample by enumerating fibers within a 100- μ m orthogonal space of an image, and multiplying that value by 100 for the 10 mm width of the entire sample.

2.4. Fourier-Transform Infrared Spectroscopy (FTIR)

FTIR was performed with a Thermo Nicolet Nexus 670 FTIR system in transmission mode. A polarized filter was used to record sample absorbance when the angle of the fiber axis was

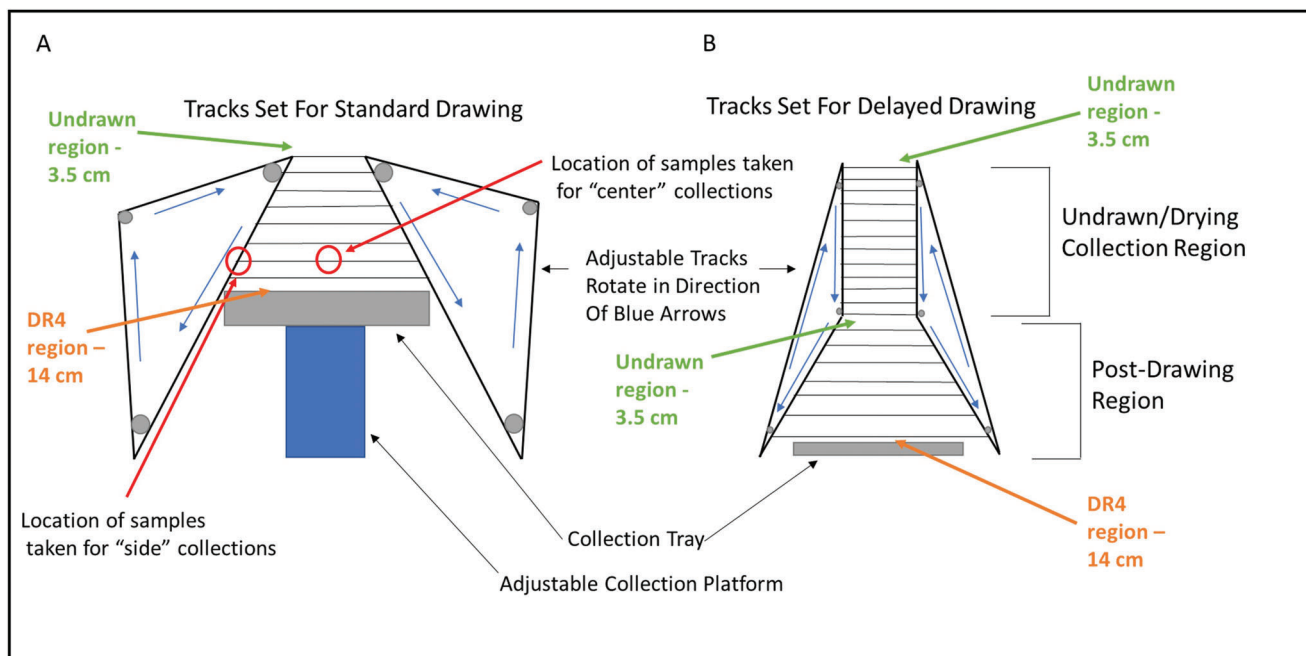


Figure 1. A) Automated track system configuration for standard drawing of electrospun nanofibers to allow for maximal solvent content while stretching. B) Delayed drawing configuration facilitates reduced solvent content during extension of electrospun nanofibers.

positioned parallel or perpendicular to polarized light. Omnic software was used to quantify sample absorbance at different peaks and polarization angles. The peak at 2240 cm^{-1} , associated with the triple bonded carbon and nitrogen group in PAN, was used to calculate Herman's orientation factor (f) where $f = 1$ means that polymer chains are perfectly aligned with respect to the fiber axis, $f = 0$ is indicative of no orientation, and $f = -0.5$ indicates that polymer chains align perfectly perpendicular with respect to the fiber axis.^[24–26] For PCL samples the wavenumbers examined were as follows: 2949, 2865, 1727, 1293, 1240, and 1170 cm^{-1} . All peaks recorded were normalized to the wavenumber 735 cm^{-1} since it is a relatively consistent peak associated with CH_2 . Relative crystallinity was computed as the ratio of the crystalline peak 1293 cm^{-1} divided by the amorphous peak at 1170 cm^{-1} . Polarized FTIR was also performed to investigate the macromolecular alignment of electrospun fibers for each draw rate/solvent system. Dichroic ratio was used as a relative measure of chain alignment for various bond vibrations that are arranged parallel to the PCL molecular backbone.

2.5. Mechanical Testing

Tensile testing was performed on samples adhered to plastic frames with inner dimensions of $10 \times 10\text{ mm}$ using a Shimadzu EZ-SX mechanical tester. The outer frames were cut after sample fixation in the device, but prior to tensile testing so that the fibers solely resisted the applied load. Samples were subjected to a constant strain rate of 5 mm min^{-1} until failure. Ultimate tensile strength, Young's modulus, ultimate tensile strain, and toughness were all obtained from the recorded force and displacement values. The sample cross-sectional area was estimated using the

following formula: $\pi/4 \times (\text{diameter})^2 \times (\text{total number of fibers})$. Diameter and fiber count values were independently measured with SEM using a matched sample taken from the same area as the one that was mechanically tested. Six replicates were produced and analyzed for all groups ($n = 6$).

2.6. Statistical Analysis

Overall group statistical analysis was carried out using SPSS software for all diameter, mechanical, and FTIR data through the use of a Kruskal–Wallis–H test. Group to group statistical analysis was performed using a Mann–Whitney test on the same data.

3. Results and Discussion

3.1. Variable Molecular Weight

The diameter of 50 000 Da (50k) PAN nanofibers were $489 \pm 120\text{ nm}$ at the point of collection at the top of the tracks (DR1). Fiber thinning during postdrawing to a draw ratio 3 (DR3) resulted in a reduction of diameter to $397 \pm 59\text{ nm}$ (Figure 2). The measured diameter of 150 000 Da (150k) PAN fibers was $575 \pm 82\text{ nm}$ prior to drawing (DR1) and $444 \pm 92\text{ nm}$ after postdrawing to DR3. Electrospun 50 and 150k PAN nanofibers had similar diameters and experienced similar percent reductions in diameter of 18.8% and 22.8%, respectively after postdrawing. These similarities indicate that the solution properties remain similar at the 50 and 150 k molecular weights. Previous reports showed that $\approx 89\text{--}98$ and 125 kDa molecular weight polyvinyl alcohol nanofibers had similar fiber diameters when electrospun

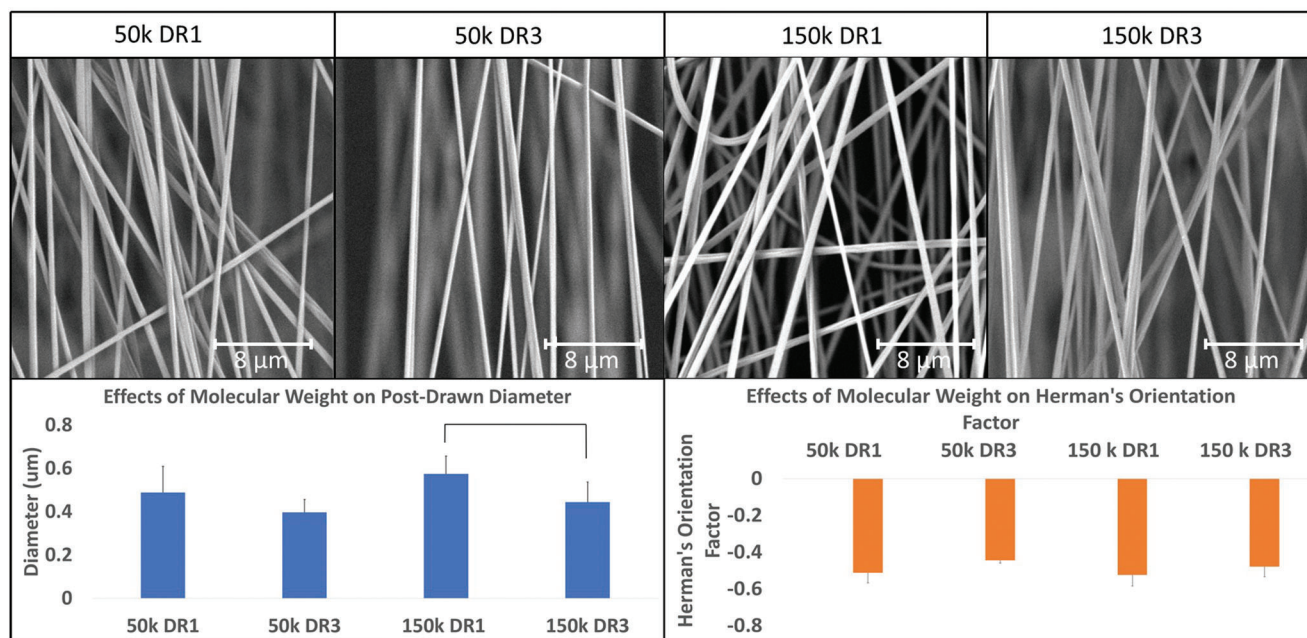


Figure 2. Effects of molecular weight on post-drawn PAN nanofiber diameter. (Top) SEM images of undrawn (DR1) and post-drawn (DR3) PAN fibers from 50 and 150k molecular weight groups. (Bottom left) Average diameter of 50k groups compared to 150k groups. (Bottom right) Herman's orientation factor for all groups. Histogram bars connected by lines have a $p < 0.01$ as determined by Mann–Whitney tests ($n = 6$). Scale bar = 8 μm.

at matched solution concentration and voltage conditions, while ≈ 146 – 186 kDa fibers spun in matched conditions consistently resulted in much larger diameters.^[27] Nanofibers with similar diameters were successfully spun from molecular number (M_n) 30–230 kDa PAN copolymer by adjusting the solutions' concentrations to match their viscosities.^[28]

The macromolecular alignment, assessed by polarized FTIR and calculated as Herman's orientation factor, of all PAN nanofibers indicated a strong perpendicular chain alignment that may be indicative of organized lamellar structures with crystalline domains oriented parallel to the fiber axis and folded polymer chains within these structures running in the direction perpendicular to the fiber axis (Figure 2). Several studies have observed that orthogonally oriented chain structures with respect to the fiber axis are representative of folded lamellar chain conformations produced within the crystalline state of a polymer.^[26,29,30] Postdrawing resulted in a small increase in orientation factor from -0.51 to -0.44 for 50k samples and -0.52 to -0.48 for 150k samples that may indicate some unfolding of perpendicular aligned chains.^[24] The molecular weight difference did not have a significant effect on electrospinning or postdrawing induced molecular reorientation.

The mechanical properties of PAN nanofibers are shown in Figure 3. For both molecular weights the ultimate tensile strength (UTS), Young's modulus (YM), and toughness increased with postdrawing, while the ultimate tensile strain decreased. The lower molecular weight nanofibers had a slightly higher as spun UTS, and both the 50 and 150k postdrawn groups had similar percent gains in UTS of 81% and 88%, respectively. In contrast, as spun fibers of both molecular weights had equivalent YM, but the 50k group demonstrated a greater percent in-

crease in YM (123%) with postdrawing compared to the 150k group (74%). An increase in UTS as a result of postdrawing is a common response which is a possible result of the reduction in fiber diameter.^[2,31–33] Diameter thinning leads to an induced confinement of the material wherein pits, cracks, and overall defects of the material are reduced, and a denser cross section is yielded, which leads to greater strength.^[25,34–40] The most significant difference ($p = 0.024$) between the 50 and 150k PAN nanofiber samples was the ultimate tensile strain that was enhanced in the more extensible postdrawn high molecular weight group (0.22) versus the postdrawn low molecular weight group (0.15). This is likely a result of the longer more stable polymer chains inherent to a relatively higher molecular weight which may be drawn further. The similarities in mechanical properties for the 50 and 150k groups are consistent with findings in the literature. Young's modulus, tensile strength, and orientation function of drawn nylon-6 films remained similar irrespective of altering molecular weight from 74 to 440k.^[41] PAN microfibers showed little change in orientation (75–76%), tensile strength (3.53–3.48 g d⁻¹), and elongation (23.4–21.2) in a molecular weight range of 165–253k.^[42] Electrospun co-polyacrylonitriles (co-PAN) demonstrated similar ultimate tensile strength (90–105 MPa) for fibers with molecular weights ranging from 30 to 110k.^[28]

The added sensitivity of electrospinning long (centimeter length scale) polymer nanofibers across a parallel track system limits the working range of molecule weights. The limited variation in morphological, macromolecular, and mechanical properties may indicate that the effects of molecular weight on these properties within these working ranges may be incremental, and warrant selecting a molecular weight based on other factors such as availability, cost, and spin-ability.

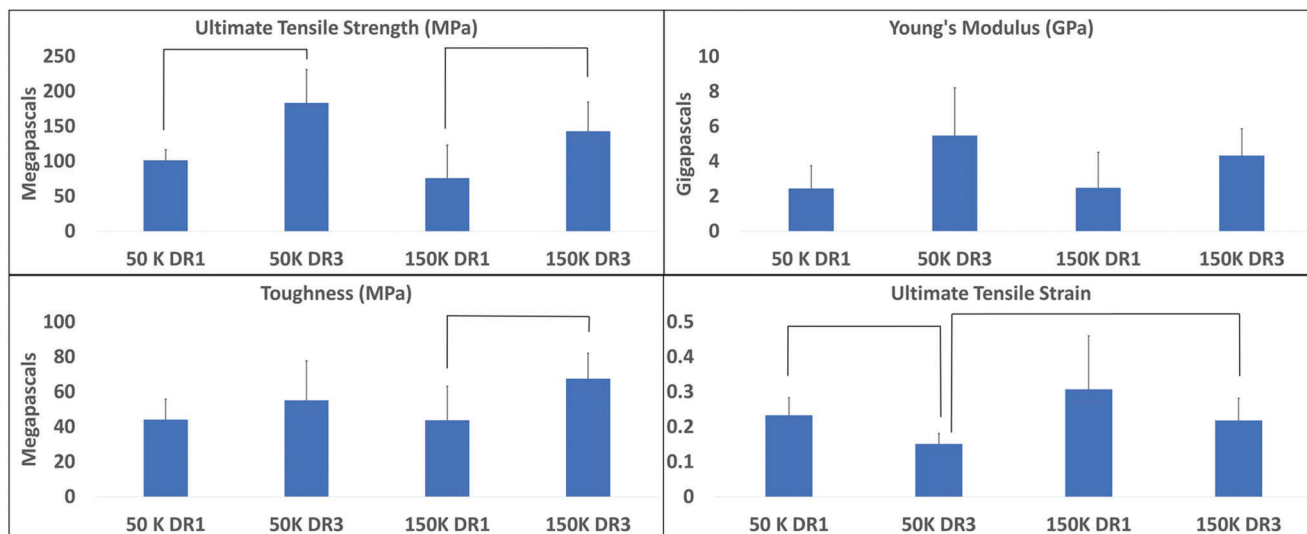


Figure 3. Effects of molecular weight on postdrawn PAN nanofiber mechanics. (Top left) Ultimate tensile strength for undrawn and drawn molecular weight groups. (Top right) Young's modulus values for all molecular weight groups. (Bottom left) Toughness for all drawn and molecular weight groups. (Bottom right) Ultimate tensile strain for all drawn and molecular weight groups observed. Histogram bars connected by lines have a $p < 0.05$ as determined by Mann–Whitney tests ($n = 6$).

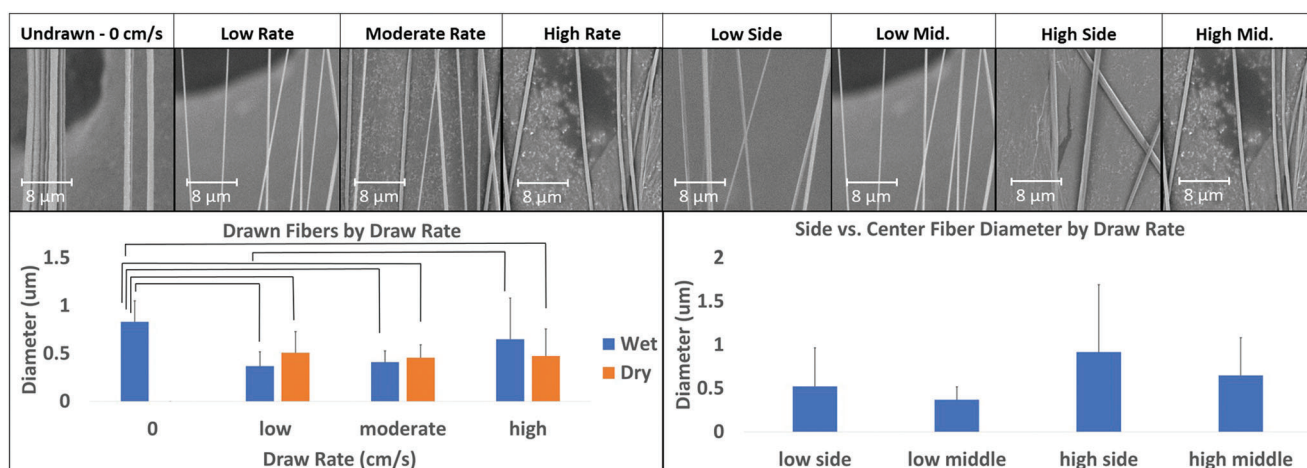


Figure 4. Influence of draw rate on post-drawn PCL diameter and uniformity. (Top left) Representative SEM images of all draw rate groups in addition to undrawn. (Top right) Representative SEM images of side and middle fiber collections at the low and high draw rate. (Bottom left) Fiber diameter for all draw rate groups including undrawn at both wet and dry-drawn collections. (Bottom right) Diameters of fibers obtained from the side and center of collections at low and high draw rates. Histogram bars connected by lines have a $p < 0.05$ as determined by Mann–Whitney tests ($n = 6$). Scale bars = $8 \mu\text{m}$.

3.2. Variable Draw Rate and Solvent Content

The diameters of polycaprolactone (PCL) nanofibers before and after postdrawing at low, medium, and high draw rates with and without a solvent drying delay are shown in **Figure 4**. The initial fiber diameter ($833 \pm 219 \text{ nm}$) decreased substantially with drawing to DR4 under all conditions. Fibers drawn after a 3 min delay, to allow solvent evaporation prior to postdrawing, had similar average fiber diameters in a range of 458–510 nm for draw rates over three orders of magnitude (0.0764 , 0.593 , and 2.74 cm s^{-1}). The diameter of fibers drawn immediately upon collection were significantly sensitive to draw rate ($p = 0.025$) with average diam-

eter increasing from 370 to 650 nm as draw rate increased over the same three orders of magnitude (0.0417 , 0.303 , 1.49 cm s^{-1}). The complexity of the system offers several possible reasons for the sensitivity of diameter to draw rate in the standard “wet” configuration: (1) Necking may occur differently at different levels of solvency resulting in different center fiber diameter (measured above the center of the fiber); (2) Collection at high speeds may have caused the large degree of variability in fiber diameter observed for the wet-high draw rate group since the residual charge on fibers previously deposited across the gap alters the electrical field and thus the stretching forces experienced by the fibers during electrospinning; (3) Fiber density changes due to porosity

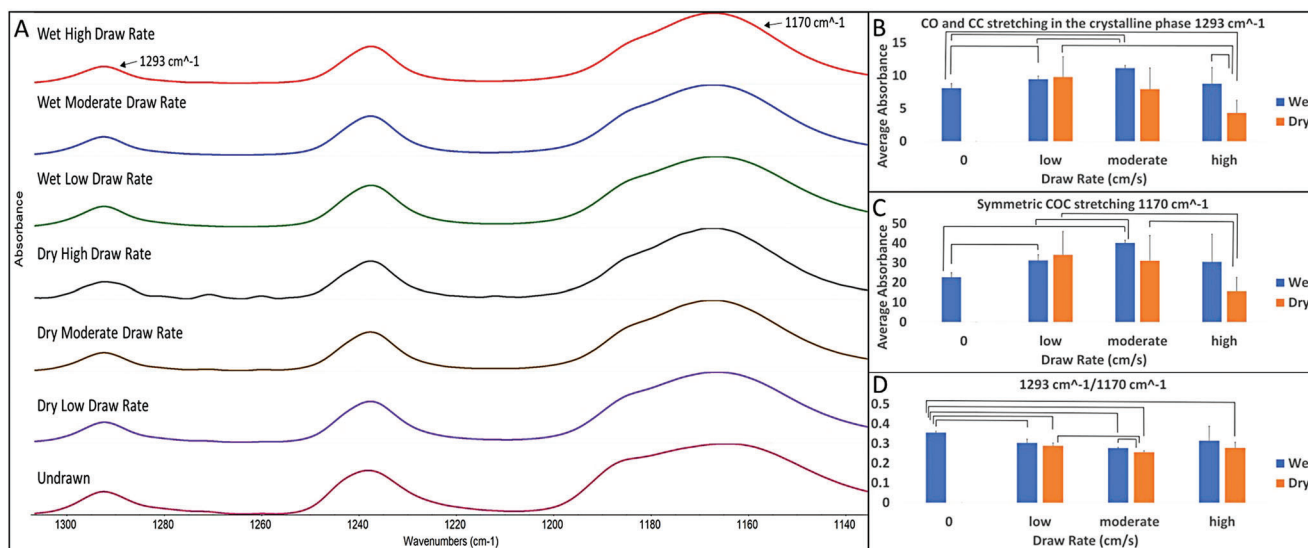


Figure 5. FTIR analysis of relative crystallinity: A) Representative FTIR spectra normalized to 1170 cm^{-1} peak height. B) Average normalized 1293 cm^{-1} peak height ($n = 6$). C) Average normalized 1170 cm^{-1} peak height ($n = 6$). D) Ratio of 1293 cm^{-1} peak height divided by 1170 cm^{-1} peak height as an indicator of total crystallinity, where larger values indicate higher relative crystalline content. Connected lines indicate $p < 0.05$. Absorbance in (B), (C) is normalized to the peak height at 735 cm^{-1} .

formation or variations in macromolecular structures that occur during curing as they are dependent on solvent content at various stages of drawing and transfer to the collection rack. However, since the volume of a 650 nm fiber is three times the volume of a 370 nm fiber and no pores were observed in SEM images, we hypothesize that it is unlikely that fiber density changes are wholly responsible for the observed dependency of fiber diameter on draw rate. Fiber uniformity experiments were performed to assess whether variations in necking geometries could be causing local diameter variation observed above. The uniformity study performed for samples processed in the standard configuration (Figure 1A, “wet” blue – Figure 4 bottom right) yielded results wherein the terminal ends of fibers produced at a low draw rate were 524 ± 443 nm while fiber diameters at the center of collection for the same draw rate were 370 ± 147 nm. For high draw rate collections fibers were recorded to be 918 ± 775 and 650 ± 432 nm for diameters observed at the side and center of deposition, respectively. The end versus center difference in diameter for low and high draw rate wet drawn fibers were both 29%, indicating that necking was observed with a similar taper in diameter for both draw rates, and is likely not the cause of diameter dependency on draw rate for “wet” drawn fibers. Thus, we hypothesize that the variable fiber deposition, and thus charge density, in the collecting area that is inherently coupled with collecting at a high draw rate is likely causing the diameter dependence. This hypothesis underscores the challenges of characterizing a system where fiber solvent content, applied electrical forces, and draw rate cannot be decoupled.

FTIR results indicated numerous changes to the chemical bond structure of PCL associated with postdrawing and sensitivity to draw rate (Figure 5; Figure S1, Supporting Information). The peaks at 1170 cm^{-1} (CO and CC stretching),^[43] 1240 cm^{-1} (asymmetric COC stretching), 1293 cm^{-1} (CO and CC stretching),^[44] 2865 cm^{-1} (symmetric CH_2 stretching), and 2949

cm^{-1} (asymmetric CH_2 stretching) all had significant differences ($p < 0.05$) in normalized absorption for postdrawn PCL nanofibers versus undrawn control and sensitivity to draw rate, which was especially prominent for “dry” groups drawn after a 3 min delay. The ratio of the peaks at 1293 and 1170 cm^{-1} were calculated for all samples as a relative indication of percent crystallinity of the samples (Figure 5D).^[45] Results indicate that drawing generally results in lower crystallinity versus undrawn controls, but a systematic dependency of crystallinity versus draw rate or solvent content was not apparent.

Polarized FTIR was utilized to evaluate the chain backbone alignment between PCL nanofibers postdrawn under different conditions (Figure 6; Figure S1E, Supporting Information). The CO and CC bonds in the PCL molecular backbone have previously been associated with two different peaks depending on whether the molecule is in the amorphous (1170 cm^{-1}) or crystalline phase (1293 cm^{-1}). Thus, the relative alignment of these two peaks in the direction of the fiber axis, quantified as dichroic ratio, is an indicator of the overall chain alignment in the amorphous and crystalline regions. Dichroic ratio was four times lower for the amorphous wavenumber versus the crystalline wavenumber in undrawn fibers. The alignment of the amorphous wavenumber was minimally affected by postdrawing for all rates and solvent contents. However, the crystalline wavenumber showed a significant drop ($p < 0.05$) in dichroic ratio for postdrawn versus undrawn fibers, and this value decreased further for “dry” drawn samples as the draw rate was increased. Greater internal stress is likely for the high draw rate fibers versus low draw rate fibers, which could be resulting in an increased disruption in the crystal alignment of the polymer chains.^[46] Overall, these results indicate that electrospinning across parallel tracks induces a high degree of polymer chain orientation with respect to the fiber axis, especially in the crystalline portions of the nanofiber. Postdrawing appears to either disrupt the process of

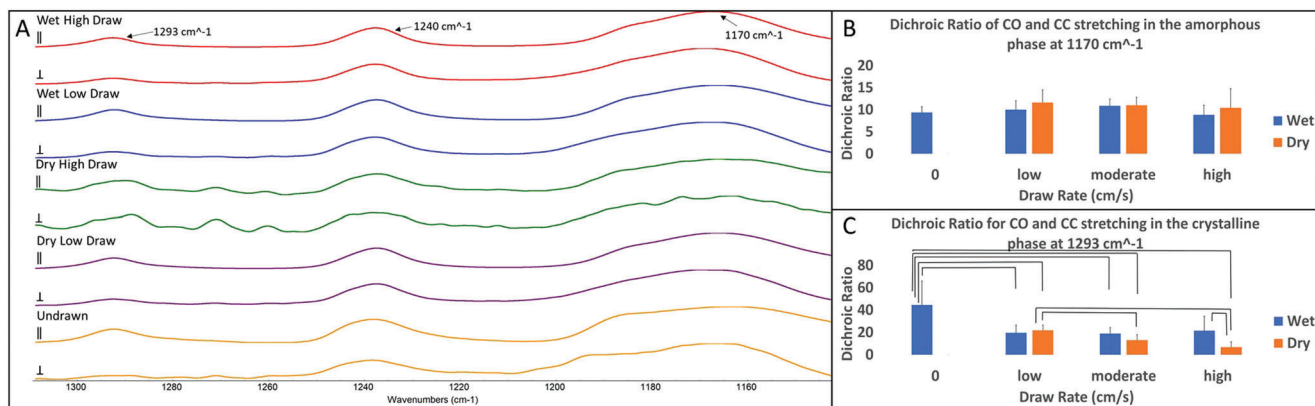


Figure 6. FTIR analysis of macromolecular alignment: A) Representative FTIR spectra taken of parallel (//) and perpendicular (⊥) polarized light with respect to the fiber axis. Spectra are normalized to the peak height at 1170 cm^{-1} . B) Average dichroic ratio at 1170 cm^{-1} ($n = 6$) serves as a relative representation of chain alignment in the amorphous regions. C) Average dichroic ratio at 1293 cm^{-1} ($n = 6$) serves as a relative representation of chain alignment in the crystalline regions.

crystallization occurring after initial collection in undrawn fibers or disorder crystals formed during electrospinning, and during the 3 min curing period (for “dry” groups). It is important to note that the crystal alignment is not always in the same orientation as the chain alignment, for example if folded chains are packed into lamellar structures, the chain alignment would be orthogonal to crystal alignment in contrast to straight chain crystals. The difference in the crystalline wavenumber alignment between “wet” and “dry” drawn samples leads us to hypothesize that enough residual solvent remains in the fibers immediately after electrospinning to significantly affect the resultant structure of processed nanofibers. A three minute drying time allows sufficient solvent evaporation to alter the postdrawing process/structure relationship, so we expect that significant curing occurs within that time period. The greater reduction in crystalline wavenumber dichroic ratio for “dry” drawn fibers with increasing draw rate demonstrates the importance of the capability to postdraw electrospun nanofibers immediately upon collection when solvent content is high. Notably, the automated track system possesses the capability to incorporate a drying step of any length of time into a continuous system by increasing/decreasing the fixed track gap portion of the device.

4. Conclusion

This study demonstrated that electrospun polymer nanofibers could be post-drawn with an automated track collector at a range of draw rates, and at different molecular weights with limited changes to the macromolecular orientation and mechanical properties. This indicates the flexibility of this manufacturing process, however, the challenges of modifying these parameters, are reflected in somewhat limited operating ranges and difficulties with fibers peeling off of the tracks for some parameter/polymer combinations. It is clear that postdrawing enhances mechanical properties overall, but observed molecular weight dependencies on tensile strength were limited. Previously mentioned reports on molecular weight dependencies on tensile strength for a similar system were conflicting, but several are in agreement with the observed results. In addition, electrospinning collection occurred

on a centimeter scale across parallel tracks, which could limit the processing range of usable molecular weight polymers that could lead to property enhancement. Although ultimate tensile strain was enhanced with increased molecular weight it is possible that the net overall effects of drawing heavier polymer chains could work to resist the alignment of these segments and impede more substantial mechanical strengthening. With respect to the parameter of draw rate, it has been shown that the high speed spinning of conventional fibers led to an inducement of crystallization,^[12] while another study demonstrated high speed spinning can reduce crystallinity, crystallization time, and molecular alignment.^[13] A reduction in molecular alignment with dry drawn fibers at increasing draw rates was present in the crystalline phase of CO and CC of the polymer in the current study which is consistent with the aforementioned findings. The importance of residual solvent content at the time of postdrawing, as a result of modulating draw rate, was highlighted by differences in macromolecular arrangement in nanofibers that were post-drawn immediately upon collection versus those given a short drying period for solvent evaporation. The role of residual solvent as well as draw rate in postdrawing indicates the value of the unique capability of automated tracks to postdraw individual nanofibers immediately upon deposition from an electrospinning jet.

Supporting Information

Supporting Information is available from the Wiley Online Library or from the author.

Acknowledgements

Research was sponsored by the National Science Foundation (NSF1653329) and the Army Research Laboratory under Cooperative Agreement Number W911NF-17-2-0227. The views and conclusions contained in this document are those of the authors and should not be interpreted as representing the official policies, either expressed or implied, of the Army Research Laboratory or the U.S. Government. This article has been contributed to by US Government contractors and their work is in the public domain in the USA.

Conflict of Interest

The authors declare no conflict of interest.

Data Availability Statement

The data that support the findings of this study are available from the corresponding author upon reasonable request. Selected raw data can be publicly accessed at Mendeley Data - DOI: <http://doi.org/10.17632/2ynzpgxckn.2>

Keywords

electrospinning, polymers, postdrawing, draw rate

Received: July 15, 2022
Revised: August 29, 2022
Published online:

- [1] M. R. Mackley, *Phys. Technol.* **1978**, 9, 13.
- [2] H. F. Giles Jr., E. M. Mount III, J. R. Wagner Jr., *Extrusion: The Definitive Processing Guide and Handbook*, William Andrew, NY, USA **2004**.
- [3] H. J. Kim, I. C. Um, *Int. J. Biol. Macromol.* **2014**, 67, 387.
- [4] R. Madurga, A. M. Gañán-Calvo, G. R. Plaza, J. M. Atienza, G. V. Guinea, M. Elices, P. A. López, R. Daza, D. González-Nieto, J. Pérez-Rigueiro, *Polymer* **2018**, 150, 311.
- [5] Y. Wang, W. Zhao, X. Wang, D. Wu, *Fibers Polym.* **2016**, 17, 1464.
- [6] Y. Termonia, P. Smith, *Macromolecules* **1987**, 20, 835.
- [7] M. Elices, *Structural Biological Materials: Design and Structure-Property Relationships*, Elsevier, Amsterdam, Netherlands **2000**.
- [8] Y. Termonia, P. Meakin, P. Smith, *Macromolecules* **1985**, 18, 2246.
- [9] J. H. Yoon, H. Avci, M. Najafi, L. Nasri, S. M. Hudson, R. Kotek, *Polym. Eng. Sci.* **2017**, 57, 224.
- [10] S. Promnil, P.-o. Numpaisal, Y. Ruksakulpiwat, *Mater. Today: Proc.* **2021**.
- [11] D. E. Chung, I. C. Um, *Fibers Polym.* **2014**, 15, 153.
- [12] R. Hufenus, Y. Yan, M. Dauner, T. Kikutani, *Materials* **2020**, 13, 4298.
- [13] A. Ziabicki, H. Kawai, *High-Speed Fiber Spinning: Science and Engineering Aspects* (Eds: A. Ziabicki, H. Kawai), John Wiley and Sons, New York **1985**, p. 511.
- [14] G. Capaccio, T. Crompton, I. Ward, *J. Polym. Sci., Polym. Phys. Ed.* **1980**, 18, 301.
- [15] T. Kanamoto, A. Tsuruta, K. Tanaka, M. Takeda, R. S. Porter, *Macromolecules* **1988**, 21, 470.
- [16] Y. Termonia, S. R. Allen, P. Smith, *Macromolecules* **1988**, 21, 3485.
- [17] D. A. Brennan, D. Jao, M. C. Siracusa, A. R. Wilkinson, X. Hu, V. Z. Beachley, *Polymer* **2016**, 103, 243.
- [18] Y. Imura, R. Hogan, M. Jaffe, *Advances in Filament Yarn Spinning of Textiles and Polymers* (Ed: D. Zhang) Elsevier, Amsterdam, Netherlands **2014**, pp. 187–202.
- [19] D. H. Reneker, A. L. Yarin, H. Fong, S. Koombhongse, *J. Appl. Phys.* **2000**, 87, 4531.
- [20] S. A. Theron, E. Zussman, A. L. Yarin, *Polymer* **2004**, 45, 2017.
- [21] A. Greiner, J. H. Wendorff, *Angew. Chem., Int. Ed.* **2007**, 46, 5670.
- [22] D. A. Brennan, A. A. Conte, G. Kanski, S. Turkula, X. Hu, M. T. Kleiner, V. Beachley, *Adv. Healthcare Mater.* **2018**, 7, 1701277.
- [23] A. A. Conte, K. Shirvani, H. Hones, A. Wildgoose, Y. Xue, R. Najjar, X. Hu, W. Xue, V. Z. Beachley, *Polymer* **2019**, 171, 192.
- [24] D. A. Brennan, K. Shirvani, C. D. Rhoads, S. E. Lofland, V. Z. Beachley, *MRS Commun.* **2019**, 9, 764.
- [25] S. F. Fennessey, R. J. Farris, *Polymer* **2004**, 45, 4217.
- [26] J. L. White, J. E. Spruiell, *Polym. Eng. Sci.* **1983**, 23, 247.
- [27] C. Akduman, E. Perrin, A. Kumabasar, A. Çay, in *Effect of molecular weight on the morphology of electrospun poly (vinyl alcohol) nanofibers*, XIIIth International Izmir Textile and Apparel Symposium April, Semantic Scholar, Seattle Washington **2014**, pp. 2–5.
- [28] G. Duan, S. Liu, H. Hou, *e-Polymers* **2018**, 18, 569.
- [29] J. R. Fried, *Polymer Science and Technology*, Pearson Education, Upper Saddle River, New Jersey **2014**.
- [30] C. R. Bohn, J. R. Schaeffgen, W. O. Statton, *J. Polym. Sci.* **1961**, 55, 531.
- [31] I. Ward, J. Sweeney, *An Introduction to the Mechanical Properties of Solid Polymers*, John Wiley & Sons, Inc., Atrium, Southern Gate, Chichester, West Sussex, United Kingdom **2004**, pp. 95.
- [32] S. Levy, *Plastics Extrusion Technology Handbook*, Industrial Press Inc, South Norwalk, Connecticut **1989**.
- [33] J. Yao, C. Bastiaansen, T. Peijs, *Fibers* **2014**, 2, 158.
- [34] R. W. Moncrieff, *Man-made Fibres Formerly entitled: Artificial fibres*, Wiley, California **1975**.
- [35] X. Wang, K. Zhang, M. Zhu, B. S. Hsiao, B. Chu, *Macromol. Rapid Commun.* **2008**, 29, 826.
- [36] E. Fitzer, *Carbon* **1989**, 27, 621.
- [37] L. Zhang, A. Aboagye, A. Kelkar, C. Lai, H. Fong, *J. Mater. Sci.* **2014**, 49, 463.
- [38] D. Sawai, Y. Fujii, T. Kanamoto, *Polymer* **2006**, 47, 4445.
- [39] J. Chen, I. Harrison, *Carbon* **2002**, 40, 25.
- [40] A. Griffith, J. J. Gilman, *Trans. ASM* **1968**, 61, 855.
- [41] M. Ito, A. Takahashi, N. Araki, T. Kanamoto, *Polymer* **2001**, 42, 241.
- [42] J.-S. Tsai, C.-H. Lin, *J. Appl. Polym. Sci.* **1991**, 42, 3045.
- [43] V. K. Khatiwala, N. Shekhar, S. Aggarwal, U. K. Mandal, *J. Polym. Environ.* **2008**, 16, 61.
- [44] A. C. Gurlek, B. Sevinc, E. Bayrak, C. Erisken, *Mater. Sci. Eng., C* **2017**, 71, 820.
- [45] Castilla-Cortázar, Vidaurre, Marí, Campillo-Fernández, *Polymers* **2019**, 11, 1099.
- [46] M. M. Shokrieh, V. A. Joneidi, R. Mosalmani, *J. Thermoplast. Compos. Mater.* **2015**, 28, 818.